

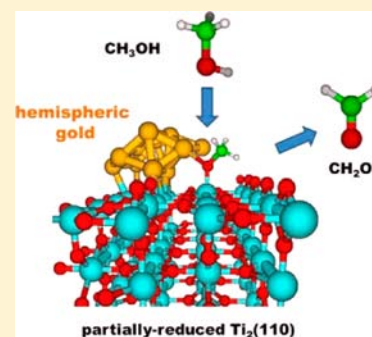
Rationale for the Higher Reactivity of Interfacial Sites in Methanol Decomposition on Au₁₃/TiO₂(110)

Sampyo Hong and Talat S. Rahman*

Department of Physics, University of Central Florida, Orlando, Florida 32816-2385, United States

S Supporting Information

ABSTRACT: Interfacial and perimeter sites have been known for their high activity in various reactions on supported gold nanoparticles. We find that the higher activity of interfacial sites in Au₁₃/TiO₂(110) toward methanol decomposition originates from charge-transfer-induced Coulomb interaction among the gold, reactant, and reducible TiO₂ support, brought about through the formation of an ionic O–Au bond between gold and methoxy in such sites, which turns the participating perimeter gold atom cationic. A direct result of such charge-transfer-induced repulsive interaction between cationic gold and positively charged C moiety of methoxy is activation of the positively charged C moiety of methoxy, as manifested by the pronounced elongation of O–C bond length and the tilting of the methoxy axis, which facilitate reaction of methoxy through C–H scission with the bridge oxygen atoms that are readily available from the reducible support. More generally, our proposed mechanism for the reactivity of the gold/TiO₂ interface should hold for oxidation of organic molecules with the structure of R–O–R', where R and R' are (saturated) hydrocarbons.



INTRODUCTION

It is now well established that gold nanoparticle (NP), in contrast to inert bulk gold, can be highly active for reactions such as CO oxidation¹ and propylene epoxidation,² even at temperatures below 300 K. Various factors responsible for this high reactivity have been proposed, including size,³ low-coordination⁴ and interfacial (perimeter) sites,^{5–9} support,¹⁰ shape/geometry,¹⁰ and gold oxidation state.^{11,12} Among them, NP size is probably the best explored. The known critical size of reactive gold NPs is ~ 3 nm.^{3,12} This size effect has been reasonably attributed to a high density of low-coordinated atoms such as those at corner and edge sites (active sites).^{4,13,14} There has also been discussion of quantum size effect: For example, gold thin films of two or three atomic layers are found to be especially reactive.^{3,15} Another factor controlling the reactivity is the interface, as demonstrated by reverse catalysts experiments which show that the interface between gold and titania is catalytically active.^{9,16} The interface naturally connects to the role of NP support; for CO oxidation on reducible oxide supports display much higher reactivity than nonreducible ones.¹⁰ On the other hand, the shape of NPs may also be a determining factor: Hemispheric, titania-supported gold NPs are found to possess a high reactivity toward propylene epoxidation.² The pioneering CO oxidation experiments^{8,10} on gold NP also find the shape to be hemispherical, making a contact angle $< 90^\circ$ as a result of reduced surface tension¹⁷ which is traceable to strong interaction of the NP with the support. As for the oxidation state (cationic) of gold, there has not been much consensus whether it is a necessary or a sufficient condition for catalytic activity (for CO oxidation)^{11,18,19} Although at first glance the proposed reactivity factors for gold NP-based CO oxidation appear to be

independent, they are in fact related and can be placed in two broad categories: (1) size (the density of active sites) and (2) interface effects (strong gold-support interaction), attributed to better and stronger mixing of the wave functions of the reactant, gold, and support atoms at the active sites.¹⁰

Given the importance of gold in nanocatalyst design and application, a question to ask is whether the activity factors summarized above could be generalized for other prototypical and technologically relevant reactions facilitated by gold NPs. In this regard, a recent coupled experimental and theoretical investigation⁵ of hydrogen oxidation on titania supported Au NPs has identified the interfacial sites as the active one. More recently the Chen group showed that in methanol decomposition on this surface, while no formaldehyde forms on pure TiO₂(110), deposition of gold NPs on this surface activates formation of formaldehyde as a principle product, important in itself for production of other valuable chemicals. Furthermore, not only does the formation of formaldehyde depend strongly on gold coverage but also such dependence correlates with the variation in the density of the available interfacial sites, pointing to the importance of these sites.²⁰ Motivated by these findings and aided by previous works on CO oxidation, we present here results of *ab initio* examination of the system surface electronic structure which trace the production of formaldehyde in methanol decomposition on gold NPs on TiO₂(110) to the special role of the interfacial sites. We find that charge transfer from gold to reaction intermediate methoxy, adsorbed at the interfacial site, activates it (methoxy) for facile formation of formaldehyde. Methoxy oxidizes interfacial gold, making it

Received: February 1, 2013

Published: April 25, 2013

cationic which subsequently leads to the high reactivity of the gold/titania interface. Our findings go beyond the proposed activation mechanism for CO oxidation on TiO₂ supported gold NPs.²¹ It consists of two parts: charge transfer from gold to molecule and repulsive interaction of cationic gold and positively charged part of molecule. The former leads to the occupation of antibonding state of molecule, as already proposed by Lie et al for O₂ activation by Au/TiO₂.²¹ The latter, causes the excitation of the positively charged part of the molecule leading to activation thereof while it stabilizes the negatively charged part of the molecule. In case of methoxy, which consists of negatively charged O and positively charged hydrocarbon (CH₃), our activation mechanism predicts excitation (activation) of the CH₃ by the repulsive potential of the cationic gold alone (apart from charge-transfer-induced occupation of the antibonding state), which is manifested by much larger elongation of O–C bond length and tilting of O–C axis. On the basis of the above argument we can also conclude that this activation mechanism is rather global in scope and applicable for oxidation of organic compounds with the structure R–O–R' (R,R' = hydrocarbons) by supported gold NPs.

THEORETICAL SECTION

Model System. Our model systems representing the Au NP, the TiO₂(110) surface and methanol are presented in Figure 1. The gold NP consists of 13 atoms, as it is small

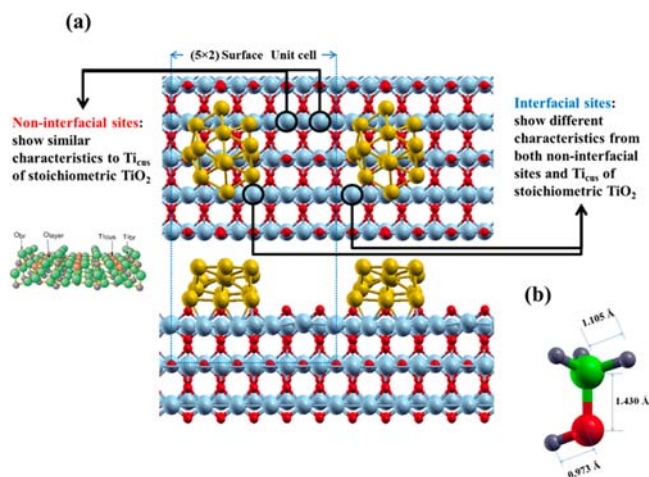


Figure 1. A schematic model of (a) Au₁₃ on a partially-reduced TiO₂(110) surface and of (b) methanol (with calculated bond lengths).

enough to be computationally feasible and large enough to provide a hemispherical shape in contact with the substrate, mimicking that seen in experiments. As is already known, the interaction of a gold NP is stronger with a TiO₂ surface with defects than that with the defect-free, stoichiometric surface.^{17,22} Thus, modeling of a relatively strong interaction of gold and TiO₂ (so as to stabilize the NP on the surface) may require some defect, such as an O vacancy as anchoring site.¹⁷ We use a (3 × 1) surface unit cell for the adsorption of methanol on the stoichiometric and fully reduced TiO₂(110), a (3 × 2) unit cell for the dissociation of methanol on the stoichiometric TiO₂(110), and a (5 × 2) surface unit cell for reaction of methanol on Au₁₃-deposited, partially reduced TiO₂(110). To make the calculations computationally feasible,

and in keeping with previous related work,²² the TiO₂(110) slabs are comprised of three trilayers (O–TiO–O). The (5 × 2) partially reduced slabs have either single or three oxygen vacancies (out of 10 O_{br} atoms) in the topmost layer, thus consisting of 60 Ti and 119 or 117 O atoms, as appropriate. All atoms in the slabs are fully relaxed in all calculations using standard techniques. An important difference between the single and triple vacancy TiO₂(110) surfaces is the formation of hemispherical gold NP in the latter, as seen in Figure 2. (In the

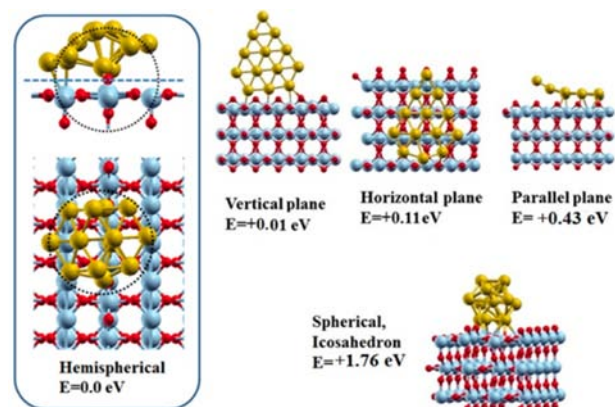


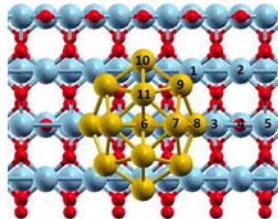
Figure 2. Adsorption of Au₁₃ cluster on the partially reduced TiO₂(110) surface with triple vacancies.

single-vacancy TiO₂(110) surface a two-dimensional NP geometry is favored instead.) As we are interested in examining the effect of factors such as support and hemispherical NP shape, we mainly use the three-vacancy TiO₂(110) slab with vacancies forming a row, for the study of methanol decomposition reaction. Although it is difficult to know the exact vacancy density in an experiment, 7–15% is considered a typical number. Higher O-vacancy density may be obtained by electron bombardment for 10 min or by Ar⁺ bombardment for 0.5 min.²³ On the other hand, aggregation of O vacancies may occur on a highly reduced TiO₂ surface, owing to O_{br}–O_{br} pairing.²⁴ Since the formation of hemispherical gold NP on TiO₂(110) surfaces is frequent,⁸ it is conceivable that the O-vacancy density employed in this study may be found at least locally on the TiO₂(110) surface. Incidentally, in another set of experiments the Au to surface defect ratio has been proposed to be about 3,^{25,26} which is not far from that in our model system. We should mention in passing that the computational modeling of the excess electron in the O vacancy can be nontrivial owing to its controversial localized character.^{27–29} We find, however, that our GGA-PBE calculations with the partially reduced, single-vacancy TiO₂(110) reproduce an upshift of 1.3 eV in the Fermi energy with respect to that in its stoichiometric surface and put the defect state at an energy of about 1.5 eV above the valence band and 0.34 eV below the conduction band, in fair agreement with experiment²⁷ and previous theory.²⁸

The 13-atom gold NP adsorbs onto the oxygen-vacancy sites in the TiO₂ surface. In Figure 1 the oxygen vacancies are hidden under the gold cluster. The model surface exposes two types of key adsorption sites for methanol: interfacial and noninterfacial, both located in the substrate (see Figure 1). While the noninterfacial sites show an adsorption geometry and reaction energetics similar to those of Ti_{cus} on the stoichiometric TiO₂ surface (see inset), the interfacial sites show quite distinct features. For optimizing the geometry of the

Table 1. Calculated Adsorption Energy of Methoxy on Au₁₃/Partially-Reduced TiO₂(110) with an Additional O Vacancy Lying Outside the Gold NP

Adsorption site	E_{ad} (eV)	Site type
1	-3.59	interfacial (Ti _{cus})
2	-3.30	non-interfacial (Ti _{cus})
3	Unstable (methoxy ends up in site 4)	Ti _{br}
4	-4.60	O-vacancy
5	Unstable (methoxy ends up in site 4)	Ti _{br}
6	-1.73	Au surface
7	-2.24	Au surface
8	-2.44	non-interfacing Au edge
9	-3.22	interfacing Au edge
10	-2.85	non-interfacing Au edge
11	-2.28	Au surface



gold NP, we prepared and fully relaxed five candidate geometries for the 13-atom cluster (Au₁₃). One is a geometry that is spherically cut from bulk, another is icosahedral, and the rest are two-dimensional (flat) geometries with different orientations with respect to the substrate. Our model of methanol with its calculated structural parameters is presented in Figure 1b. The calculated bond lengths of O–H, C–O, and C–H (0.973, 1.430, and 1.105 Å, respectively) and angle (\angle COH) (108.3°) are in close agreement with experiment (0.963, 1.421, 1.101 Å and 108.0°, respectively)^{30,31}

Details of DFT Calculations. We have performed scalar-relativistic, nonspin polarized density functional theory (DFT) calculations³² to find the transition state and activation energy barriers for the oxidation of methanol on Au₁₃/TiO₂(110), using the climbing image nudged elastic band method.³³ We have further used the Bader analysis^{34,35} to obtain the charge-density redistribution for the involved species. In the DFT method, as implemented in the Vienna Ab-Initio Simulation Package,^{36,37} the Kohn–Sham wave functions are expanded in the plane-wave basis with a kinetic-energy cutoff of 400 eV and electron/ion interactions described by the projector-augmented wave method.³⁸ For exchange–correlation energy, we used the Perdew–Burke–Ernzerhof (PBE) functional.³⁹ For the sampling of the Brillouin zone, we employed a (3 × 3 × 1) *k*-point grid for (5 × 2) surface unit cell using the Monkhorst–Pack method,⁴⁰ which produces 5 irreducible special *k*-points. With this chosen *k*-point grid, we employed the Methfessel–Paxton method⁴¹ for Fermi-level smearing with a value of 0.2 eV, which is estimated to induce an error in the calculated total energy of only 0.2 meV per atom or less. We set the threshold for electronic energy convergence to 1 × 10^{−4} eV and that for structural relaxation to 1 × 10^{−2} eV/Å. For structural relaxation, we used the standard quasi-Newtonian algorithm. Adsorption energy of a specie is calculated as follows: $E_{ad}(\text{specie}) = E(\text{specie}/\text{Au}/\text{TiO}_2) - E(\text{Au}/\text{TiO}_2) - E(\text{specie})$. For adsorption energy of gold NP, we use $E_{ad}(\text{NP}) = E(\text{NP}/\text{TiO}_2) - E(\text{TiO}_2) - E(\text{NP})$.

RESULTS AND DISCUSSION

Geometry of Gold NP on Partially-Reduced TiO₂(110).

Unsupported Au₁₃ takes a two-dimensional (flat) geometry in free space and an icosahedral if it is ligated.⁴² However, neither is a preferred structure when Au₁₃ adsorbs on the 30% reduced TiO₂(110) surface. During relaxation the 13-atom cluster (Au₁₃

spherically cut from bulk) takes the hemispherical geometry on the 30% reduced TiO₂(110) surface^{2,43} depicted in Figure 2, and has adsorption energy of −2.9 eV (per cluster). Note that the vertical 2-dimensional geometry is the next preferred. Overall, the trends shown in Figure 2 indicate that the NP geometry is such that it maximizes Au–O_{vac} and Au–Ti_{cus} bond strengths as compared to Au–Au and Au–O_{br}, i.e., we get the following bond order: Au–O_{vac} > Au–Ti_{cus} > Au–Au > Au–O_{br}.

On a partially reduced TiO₂(110) surface with only a *single* O vacancy (1 in 10 O_{br} sites), on the other hand, the hemispherical shape of gold NP in Figure 2 is no longer favored; instead, a two-dimensional (flat) geometry of Au₁₃ (similar to that of the horizontal plane NP in Figure 2) is the most stable¹⁷ among those considered here, though its binding to that surface is weaker (−1.9 eV) than that on the three-vacancy TiO₂ surface.

Leaving aside the vertical two-dimensional NP, which, despite its wealth of peripheral atoms, has only 3 points of contact with the support, none of which is Ti_{cus}, it is instructive to compare the remaining two most favored geometries of the Au₁₃ NP. Both the lower energy flat geometry, for example, the horizontal plane in Figure 2 and the hemispherical one (also in Figure 2), interface with the support at 4 Ti_{cus} sites. It is true that the flat one exhibits more low-coordinated atoms than the hemispheric one, i.e., 10, with an average coordination of 3.2, as opposed to 8, with an average coordination of 3.7. But, since the hemispherical geometry covers less area of the TiO₂(110) surface than does the flat one by a ratio of 2:6, the density of interfacial sites available to it is three times greater than the density of interfacial sites at the disposal of the other. Thus, if the interface is the controlling parameter, then hemispherical gold NPs can be expected to be more active than the other for catalytic reactions, independent of the fact that the hemispherical one happens to be the most energetically favored of the geometries considered here.

Energetics of Methanol at Partially-Reduced TiO₂(110) Surfaces.

Now let us turn to the adsorption energetics of methanol at the partially reduced (30% vacancy) TiO₂(110) surface in Figure 1. It is already known that the O–H bond of methanol breaks either spontaneously on O-rich and fully reduced TiO₂(110) surfaces or with a small activation energy on the stoichiometric surface.^{37,38} We find that there is also no barrier for O–H scission in methanol when it adsorbs

in the O-vacancy site on a fully reduced $\text{TiO}_2(110)$ surface or when it reacts with oxygen species adsorbed on top of the terminal Ti_{cus} on the stoichiometric $\text{TiO}_2(110)$ surface. Furthermore, the O–H scission barrier is only 0.12 eV on the stoichiometric surface, in close agreement with previous theoretical results which lie in the range of 0.05³⁷ and 0.11 eV.³⁸ The resulting intermediate, methoxy, is the active species of methanol on $\text{TiO}_2(110)$. Our calculated adsorption energy for methoxy at the various possible sites is presented in Table 1. Note that for the results presented in Table 1, we have included an additional O vacancy which lies outside the gold NP (three O vacancies sit underneath the gold NP) on the $\text{TiO}_2(110)$ surface for comparison of adsorption energies between various sites summarized below. For all other calculations we use the 30% reduced $\text{TiO}_2(110)$ surface without this additional O vacancy. We thus recalculate the adsorption energies of methoxy on the 30% reduced $\text{TiO}_2(110)$ surface (without the additional O vacancy) and present it together with those of methanol and formaldehyde in Table 2.

Table 2. Calculated Adsorption Energy of Methanol, Methoxy and Formaldehyde on $\text{Au}_{13}/30\%$ -reduced $\text{TiO}_2(110)$ ^a

adsorption site	adsorption species	E_{ad} (eV)	site type
1	methanol	−1.37	interfacial (Ti_{cus})
2	methanol	−1.14	noninterfacial (Ti_{cus})
1	methoxy	−3.66	interfacial (Ti_{cus})
2	methoxy	−3.41	noninterfacial (Ti_{cus})
1	formaldehyde	−1.69	interfacial (Ti_{cus})
2	formaldehyde	−0.91	noninterfacial (Ti_{cus})

^aWith no additional O vacancy lying outside of gold NP.

It is clear from Table 1 that the O-vacancy site is the preferred adsorption site for methoxy on the $\text{Au}/\text{TiO}_2(110)$ surface. From such a site we find methoxy to desorb as methyl (CH_3) with a calculated desorption energy of 1.94 eV, in good agreement with measured desorption of methyl at 640 K.²⁰ Since experiments find formaldehyde in addition to methyl, the question is: Where do the latter originate on the $\text{Au}/\text{TiO}_2(110)$ surface? To answer this question we turn to the next preferred methoxy adsorption site which is the interfacial one (entry 1 in Table 1). It is favored over the noninterfacial site by 0.3 eV (Table 1) or 0.25 eV (Table 2). In this hierarchy of adsorption sites, it is interesting to note that the next one is the *interfacial* gold atom (entry 9 in Table 1) that has an adsorption energy of −3.22 eV (Table 1), just about 0.4 eV less than that for the most preferred site—a fact that points to the markedly enhanced adsorption in the interfacial region. Adsorption of methoxy on the remaining surface sites of the gold NP is not favored, not even in the low-coordinated perimeter sites (entries 8 and 10 in Table 1). As for the reaction product formaldehyde,⁴⁴ its preferred adsorption site is also the interfacial one by a large margin (−1.69 vs −0.91 in Table 2).

Adsorption Geometry and Activation Energy Barriers for Methoxy. We present the adsorption structure of methoxy in Figure 3 and that of its decomposed species, formaldehyde and hydroxyl, in the noninterfacial and interfacial sites in Figure 4. The relevant structural parameters are laid out in Table 3.

We see remarkable changes in the structure of methoxy when the adsorption site changes from noninterfacial to interfacial: (1) formation of an Au–O bond; (2) much-larger tilting of (methoxy) axis; and (3) elongation of the O–Ti and O–C

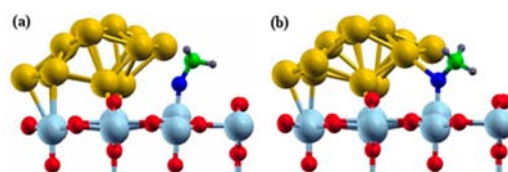


Figure 3. Schematics of methoxy adsorption on $\text{Au}_{13}/30\%$ -reduced $\text{TiO}_2(110)$ surface at: (a) a noninterfacial and (b) an interfacial site. We use light-blue spheres for Ti, yellow for Au, red for support, dark-blue for molecular O, green for C, and gray for H.

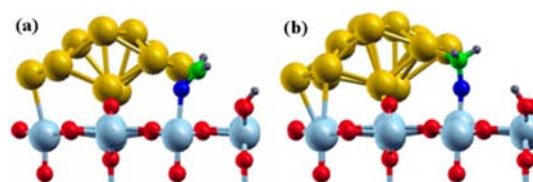


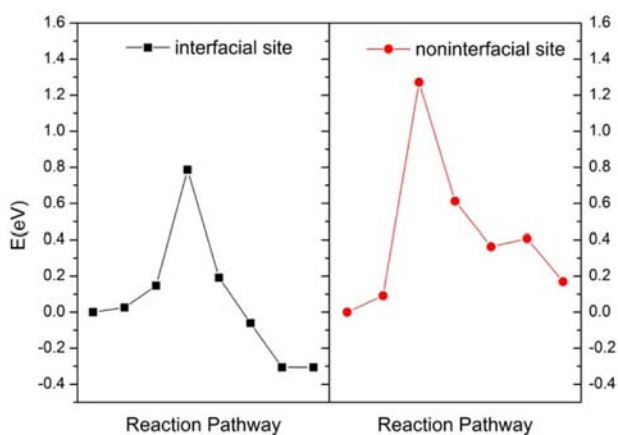
Figure 4. Schematics of formaldehyde and hydroxyl adsorption on $\text{Au}_{13}/30\%$ -reduced $\text{TiO}_2(110)$ surface at: (a) a noninterfacial and (b) an interfacial site. Color coding is the same as in Figure 3.

bond lengths. The elongation of the O–Ti bond indicates a weaker binding between the O and Ti atoms at the interfacial site, probably owing to the formation of the O–Au bond. The formation of the O–Au bond, on the one hand, weakens the O–C bond but, on the other, stabilizes adsorption in the interfacial site (than that in the noninterfacial one). As we shall see, methoxy reaction is promoted by the more pronounced tilting of the methoxy axis in the interfacial site. To be precise, the tilting angle $\theta(\text{Ti}–\text{O}–\text{C})$ in Table 3 when methoxy adsorbs at the interfacial site is 134° , while it is 150° when adsorption takes place at the noninterfacial site. Accordingly, the shorter interatomic distance between the H and O_{br} is at the interfacial site (2.04 Å compared to 2.52 Å at the noninterfacial site). This substantial reduction of interatomic bond length, $d(\text{H}–\text{O}_{\text{br}})$, indicates enhanced electrostatic attraction between the cationic H of the methoxy and anionic O_{br} .

Our calculated energy barrier for the decomposition of methoxy to formaldehyde via C–H scission is 0.78 eV at the interfacial site and 1.29 eV at the noninterfacial site, as shown in Figure 5. This relative ease in C–H scission accounts for the higher activity of interfacial site over noninterfacial one. Interestingly, since the adsorption energy of formaldehyde at the interfacial site (−1.69 eV) is much higher than that at the noninterfacial one (−0.91 eV), the rate-limiting step for production of formaldehyde is desorption in the interfacial site and C–H scission in the noninterfacial site. In terms of the overall reaction rate, the lower desorption barrier of formaldehyde at the noninterfacial site may suggest a higher activity (than the interfacial site) for this site. But apart from the preference of both methanol and methoxy for the interfacial site (Table 2), one should also take into consideration their diffusion barriers from the noninterfacial to the interfacial site, which we find to be 0.35 (methanol) and 0.89 eV (methoxy). These factors imply that formaldehyde forms mainly at the interfacial site, since methoxy adsorbed in the noninterfacial site diffuses to the interfacial site (which requires 0.89 eV) rather than undertaking C–H scission in the noninterfacial site (which needs 1.29 eV). These formaldehyde molecules desorb at 589 K (according to our simulated desorption of formaldehyde using kinetic Monte Carlo simulations) in good agreement with the measured desorption temperature of 535 K

Table 3. Bond Length and Angle of Methoxy and Formaldehyde on Au₁₃/30%-Reduced TiO₂(110) Surface

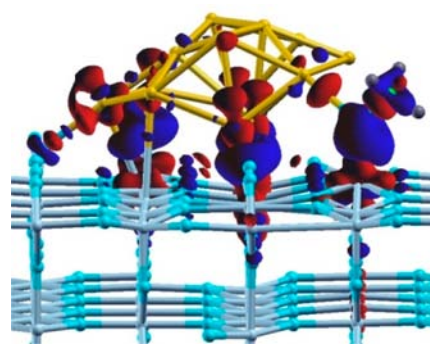
species	adsorption site	$d(\text{O}-\text{Ti})$	$d(\text{O}-\text{C})$	$d(\text{C}-\text{H})$	$d(\text{O}-\text{Au})$	$\theta(\text{Ti}-\text{O}-\text{C})$	$\theta(\text{Ti}-\text{O}-\text{Au})$
methoxy	[gas phase]	—	1.345	1.120	—	—	—
methoxy	noninterfacial (Figure 3a)	1.778	1.410	1.103	—	152°	—
				1.101			
				1.101			
methoxy	interfacial (Figure 3b)	1.840	1.435	1.101	2.546	134°	120°
				1.101			
				1.098			
formaldehyde	noninterfacial (Figure 4a)	2.0203	1.226	1.108	—	140°	—
				1.110			
formaldehyde	interfacial (Figure 4b)	1.821	1.360	1.104	—	170°	—
				1.104			

Figure 5. Calculated energy barrier of methoxy decomposition at interfacial and noninterfacial sites on Au₁₃/30%-reduced TiO₂(110).

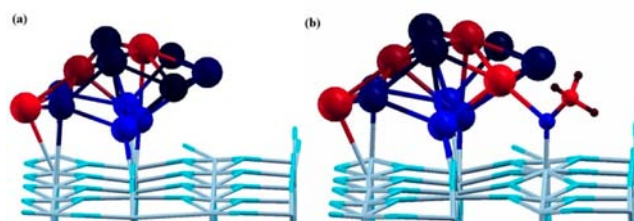
from a TiO₂(110) surface with 0.25 ML gold NP.²⁰ On the other hand, methoxy can, in principle, convert to methyl via O–C scission. However, our calculated barrier for breaking O–C bonds of methoxy and desorbing as CH₃ is 2.56 eV in the interfacial site and 3.29 eV in the noninterfacial site. Thus, CH₃ formation through direct O–C scission at the non-O-vacancy sites is not plausible. Therefore, every methoxy adsorbed in the nondefect sites (i.e., in the interfacial and noninterfacial Ti_{cus} sites) is predicted to convert to formaldehyde instead of CH₃. In sum, the two prominent features of the methoxy adsorption in the interfacial site are the formation of the Au–O bond and the elongation (weakening) of the O–C bond. Our calculations predict that the dominant channel for the formation of formaldehyde is the interfacial site.

Charge Transfer at the Interfacial Sites. The question then arises: What particular electronic property of the interfacial site causes the marked differences described above? To address this point we examine in detail the bond formation at the interfacial site. We present the charge density differences within the system in Figure 6, which plots $\rho(x,y,z) = \rho[\text{methoxy}/\text{Au}_{13}/\text{TiO}_2(110)] - \rho[\text{TiO}_2(110)] - \rho[\text{Au}_{13}] - \rho[\text{methoxy}]$, where methoxy, Au₁₃, and TiO₂(110) retain the structures they exhibit in the methoxy/Au₁₃/TiO₂(110) system.

We clearly see a strong mixing of the charge densities (representing wave functions) of reactants, gold NP, and support such that charge accumulates in the methoxy at the interfacial site (blue region)—particularly in the O atom of the methoxy and also in the C moiety of the methoxy—while charge depletes in the Au atom that is bonded to the O atom (red region). This charge redistribution indicates that through

Figure 6. Charge-difference plot of methoxy adsorbed at the interfacial site on Au₁₃/30%-reduced TiO₂(110). Isosurface charge density is plotted with the iso-value = $\pm 0.03e/\text{\AA}^3$. Blue and red represent charge accumulation and depletion, respectively. Light-blue indicates Ti, yellow Au, cyan O, green C, and gray H.

the formation of the Au–O bond, the Au atom bonded to the O atom of methoxy donates electron density to methoxy, especially to its O atom, with the result that the involved Au atom becomes positively charged (cationic), as confirmed by our Bader analysis presented in Figures 7 and 8.

Figure 7. Oxidation state of gold atoms (and methoxy molecule) (a) before and (b) after methoxy adsorption at the interfacial site on the partially reduced TiO₂(110) surface. Red, black, and blue represent positive, neutral, negative charge, respectively, while relative brightness indicates magnitude of the charge. The brightest blue and red, respectively, represent $-0.27e$ and $+0.1e$ in case of gold and $-0.9e$ and $+0.33e$ in case of methoxy, with respect to their neutral atomic charge.

Before methoxy adsorption (Figure 7a), most gold atoms are neutral, except for a few on the upper surface and left edge of the NP (which are cationic) and those on the bottom surfaces (which are anionic). Note that the three central gold atoms of the NP, which are strongly bonded to O vacancies, are all anionic.^{22,45,46} Upon methoxy adsorption in the interfacial site (Figure 7b), we see hardly any noticeable change in the atomic charge of the gold atoms except for the dramatic one in the

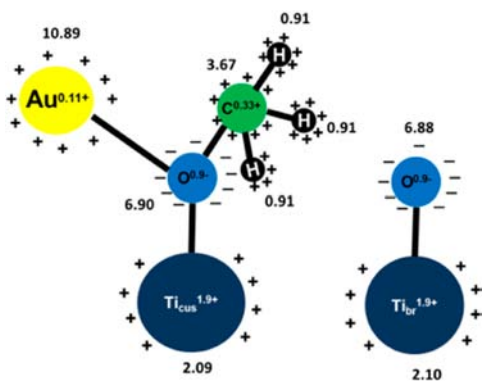


Figure 8. Bader charge of gold, methoxy, and support at the interfacial site.

interfacing gold atom that is directly bonded to methoxy. This low-coordinated interfacial gold atom donates a partial electron ($\approx 0.11e$) to the methoxy adsorbed at the interfacial site. On the whole, the gold NP donates $0.15e$ to methoxy (TiO_2 also donates $0.17e$ to methoxy). From the overall charge distribution analysis we find that the oxygen of the methoxy acquires a net excess charge of $0.9e$ (Figure 8). It is thus clear that the O–Au bond so formed is ionic and that methoxy has oxidized the interfacial gold and TiO_2 support.²⁰ As for the C moiety of the methoxy, it receives $0.13e$ beyond what it possessed in the gas phase. However, it remains positively charged: the C atom by $+0.33e$ (Figure 8) and the H atoms by $+0.09e$. Since the C and H atoms of the methoxy at the interfacial site are also positively charged there is a net repulsive interaction between the Au atom and the C moiety. It is this repulsion that causes the aforementioned large tilting of the C–O axis of methoxy adsorbed at an interfacial site. This repulsive interaction activates methoxy for C–H scission. Since the C moiety is in the electric field of the positive Au atom, its energy level will shift up while that of negatively charged O atom will shift down, thereby stabilizing the O atom (less reactive) but unstabilizing the positively charged C moiety (more reactive). The elongation of O–C bond length is thus a result of activation of methoxy by the repulsive potential of the cationic gold. In sum, charge-transfer induced activation of methoxy (by the repulsive potential of the cationic gold) together with the enhanced H–O_{br} interaction by the large tilting of methoxy axis contribute to reduction of the energy barrier for C–H scission reaction in the interfacial site. The effectiveness of the mechanism proposed above can be estimated quantitatively by examining the change of the energy barrier for O–C and C–H scission from noninterfacial site to interfacial site. (The O–C and C–H scission in the noninterfacial site do not involve the proposed activation process.) The relative energy barrier change is -0.73 eV (from 3.29 to 2.56 eV) for O–C scission and -0.51 eV (from 1.29 to 0.78 eV) for C–H scission. Thus, the proposed mechanism could cause a reduction of about 20–40% of the nonactivated energy barriers or 0.5 – 0.7 eV, which can change reaction kinetics completely. Note that the above mechanism for the activation of gold/ TiO_2 interface is quite general and may be applied for the oxidation of organic molecules with the structure of R–O–R', where R and R' are (saturated) hydrocarbons. For methoxy, R = CH_3 .

Note also that in the case of formaldehyde, its geometry in the interfacial site (Figure 4b) is radically different from that of methoxy in the interfacial site (Figure 3a). The gold–

formaldehyde bond is not via Au–O, as in the case of gold–methoxy, but via Au–C. The charge-transfer arguments discussed above also do not apply to the case of formaldehyde, since Au–C bond is more covalent (charge sharing) than ionic (charge transfer). The strong binding of C moiety to Au indicates that the C moiety is stable (inactive).

It is instructive to examine the effect of O-vacancy density on the overall charge transfer among gold and TiO_2 , as summarized in Figure 9. (For these calculations we used the

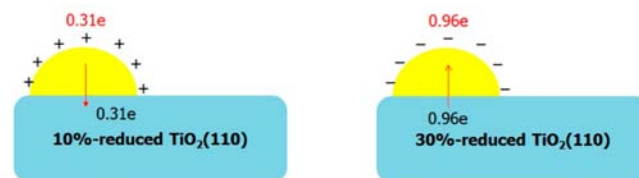


Figure 9. Effect of O-vacancy density on charge transfer among gold and support in the interfacial site.

same hemispherical Au_{13} geometry for both TiO_2 surfaces, although this is not the lowest energy geometry in the 10% reduced case.) First, the direction of charge transfer depends on the O-vacancy density (Figure 9). While in the 10% O-vacancy density case (left in Figure 9), gold on average donates charge to TiO_2 , in the 30% O-vacancy density case (right in Figure 9), gold receives it. Since charge transferred to gold can be used to facilitate reactions by gold, higher vacancy density may be more favorable for gold reactivity. Second, the vacancy density also affects the amount of charge transfer: $0.31e$ for 10% vacancy density and $0.96e$ for the 30% vacancy density case. Third, the amount of transferred charge affects the strength of the interaction of gold NP and TiO_2 : adsorption energy of Au_{13} NP in the 30% vacancy case is -2.9 eV but that of Au_{13} in 10% vacancy density case -1.9 eV. The more the charge transfer, the stronger is the binding. This stronger binding of gold in the 30% vacancy density case results in the formation of a catalytically active hemispherical geometry of Au_{13} .

Oxidation of gold during catalytic reactions that we find here is actually a more general phenomenon and not restricted to TiO_2 as support or to methanol reaction. Cationic gold has been reported with various supports, such as CeO_2 ,⁴⁷ MgO ,¹¹ and Fe_2O_3 ⁴⁸ for CO oxidation. In case of CO oxidation on Au/ TiO_2 , while it is debated whether CO adsorbs on the surfaces of gold nanoparticle or on the surfaces of TiO_2 , there is a consensus that O_2 adsorbs on the surfaces of TiO_2 and that the reaction of CO and O_2 to form CO_2 mainly occurs in the interfacial sites.^{16,21,49,50} Cationic gold was proposed to induce strong binding of gold NP with support⁵⁰ and create active gold-oxide at the gold/support interface.^{51,52} In view of the mechanism we propose here, which involves charge-transfer-induced enhanced electrostatic interaction followed by activation of the reactant, it is the charge transfer from gold to oxygen that creates the strong electrostatic attraction between the two, thereby weakens the O_2 internal bond and activates O_2 leading to the formation of gold-oxide layer. Indeed, our analysis is in accord with the proposal that charge transferred from gold to O_2 activates interfacial O_2 for CO oxidation.²¹ Thus, while there are differences in the specifics of methanol and CO oxidation on $\text{TiO}_2(110)$, there is an inherent similarity in the role of the interfacial sites.

CONCLUSION

In summary, we have shown that charge donation by gold has an obvious impact on the geometry and reaction of methoxy. First of all, it induces strong binding between the gold and the methoxy (oxygen). Second, it weakens the molecular O–C bond. Third, it brings about a repulsive interaction between gold and the C moiety of methoxy thus unstabilizing (activating) the positively charged H atoms and also causing tilting of the molecule's axis, which enhances H–O_{br} attraction. Together, these three effects substantially enhance reactivity of methoxy toward C–H decomposition. As for the active sites, our analysis defines them as those that induce catalytically more advantageous charge redistribution among reactants, catalysts, and support. In doing so, they significantly enhance the interaction of catalysts and reactants. In the case of methoxy decomposition on Au/TiO₂(110), these sites are interfacial sites, whose density is highest with hemispherical gold.

ASSOCIATED CONTENT

Supporting Information

DFT energies and coordinates of methanol, methoxy, and formaldehyde (gas phase, nonspin polarized). This material is available free of charge via the Internet at <http://pubs.acs.org>.

AUTHOR INFORMATION

Corresponding Author

Talat.Rahman@ucf.edu

Notes

The authors declare no competing financial interest.

ACKNOWLEDGMENTS

We thank D. A. Chen for kindly sharing her data on methanol decomposition on Au/TiO₂(110) with us and for helpful discussions and comments on this topic. We are grateful to Lyman Baker for careful reading of the manuscript and constructive comments. This work was supported in part by the Department of Energy, Basic Energy Sciences (DE-FG02-07ER15842). The DFT calculations were performed using the computing resources at the Texas Advanced Computing Center (TACC), the National Energy Research Scientific Computing Center (NERSC), the Center for Nanoscale Materials (CNM) of the Argonne National Laboratory, and at STOKES, and the high-performance computational facility at UCF.

REFERENCES

- (1) Haruta, M.; Kobayashi, T.; Sano, H.; Yamada, N. *Chem. Lett.* **1987**, 405.
- (2) Hayashi, T.; Tanaka, K.; Haruta, M. *J. Catal.* **1998**, *178*, 566.
- (3) Valden, M.; Lai, X.; Goodman, D. W. *Science* **1998**, *281*, 1647.
- (4) Janssens, T.; Clausen, B.; Hvolbæk, B.; Falsig, H.; Christensen, C.; Bliigaard, T.; Nørskov, J. *Top. Catal.* **2007**, *44*, 15.
- (5) Green, I. X.; Tang, W.; Neurock, M.; Yates, J. T., Jr. *Angew. Chem., Int. Ed.* **2011**, *50*, 10186.
- (6) Mavrikakis, M.; Stoltze, P.; Nørskov, J. K. *Catal. Lett.* **2000**, *64*, 101.
- (7) Iizuka, Y.; Tode, T.; Takao, T.; Yatsu, K.-i.; Takeuchi, T.; Tsubota, S.; Haruta, M. *J. Catal.* **1999**, *187*, 50.
- (8) Haruta, M.; Tsubota, S.; Kobayashi, T.; Kageyama, H.; Genet, M. J.; Delmon, B. *J. Catal.* **1993**, *144*, 175.
- (9) Rodriguez, J. A.; Ma, S.; Liu, P.; Hrbek, J.; Evans, J.; Pérez, M. *Science* **2007**, *318*, 1757.
- (10) Haruta, M. *CATTECH* **2002**, *6*, 102.
- (11) Guzman, J.; Gates, B. C. *J. Am. Chem. Soc.* **2004**, *126*, 2672.
- (12) Bond, G. C.; Thompson, D. T. *Gold Bull.* **2000**, *33*, 41.
- (13) Lemire, C.; Meyer, R.; Shaikhutdinov, S.; Freund, H.-J. *Angew. Chem., Int. Ed.* **2004**, *43*, 118.
- (14) Lopez, N.; Janssens, T. V. W.; Clausen, B. S.; Xu, Y.; Mavrikakis, M.; Bliigaard, T.; Nørskov, J. K. *J. Catal.* **2004**, *223*, 232.
- (15) Herzing, A. A.; Kiely, C. J.; Carley, A. F.; Landon, P.; Hutchings, G. J. *Science* **2008**, *321*, 1331.
- (16) Molina, L. M.; Hammer, B. *Appl. Catal., A* **2005**, *291*, 21.
- (17) Lopez, N.; Nørskov, J. K.; Janssens, T. V. W.; Carlsson, A.; Puig-Molina, A.; Clausen, B. S.; Grunwaldt, J. D. *J. Catal.* **2004**, *225*, 86.
- (18) Chen, M. S.; Goodman, D. W. *Catal. Today* **2006**, *111*, 22.
- (19) Chen, M. S.; Goodman, D. W. *Chem. Soc. Rev.* **2008**, *37*, 1860.
- (20) Tenney, S. A.; Cagg, B.; Levine, M.; He, W.; Manandhar, K.; Chen, D. A. *Surf. Sci.* **2012**, *606*, 1233.
- (21) Liu, Z.-P.; Gong, X.-Q.; Kohanoff, J.; Sanchez, C.; Hu, P. *Phys. Rev. Lett.* **2003**, *91*, 266102.
- (22) Pabisiaik, T.; Kiejna, A. *Phys. Rev. B* **2009**, *79*, 085411.
- (23) Farfan-Arribas, E.; Madix, R. J. *Surf. Sci.* **2003**, *544*, 241.
- (24) Thompson, S. J.; Landau, D. P.; Lewis, S. P. *Phys. Procedia* **2010**, *7*, 103.
- (25) Wahlström, E.; Lopez, N.; Schaub, R.; Thostrup, P.; Rønnow, A.; Africh, C.; Lægsgaard, E.; Nørskov, J. K.; Besenbacher, F. *Phys. Rev. Lett.* **2003**, *90*, 026101.
- (26) Wendt, S.; Schaub, R.; Matthiesen, J.; Vestergaard, E. K.; Wahlström, E.; Rasmussen, M. D.; Thostrup, P.; Molina, L. M.; Lægsgaard, E.; Stensgaard, I.; Hammer, B.; Besenbacher, F. *Surf. Sci.* **2005**, *598*, 226.
- (27) Sakai, Y.; Ehara, S. *Jpn. J. Appl. Phys.* **2001**, *40*, L773.
- (28) Morgan, B. J.; Watson, G. W. *J. Phys. Chem. C* **2009**, *113*, 7322.
- (29) Di Valentin, C.; Pacchioni, G.; Selloni, A. *J. Phys. Chem. C* **2009**, *113*, 20543.
- (30) Lide, D. *Handbook of Chemistry and Physics*, 74th ed.; CRC Press: Boca Raton, FL, 1994.
- (31) Pople, J. A.; Hehre, W. J.; Radom, L.; Schleyer, P. v. R. *Ab initio Molecular Orbital Theory*, 5th ed.; Wiley: New York, 1986.
- (32) Hohenberg, P. K.; W. *Phys. Rev.* **1964**, *136*, B864.
- (33) Henkelman, G.; Uberuaga, B. P.; Jónsson, H. *J. Chem. Phys.* **2000**, *113*, 9901.
- (34) Bader, R. F. W. *Atoms in Molecules: A Quantum Theory*; Oxford University Press: New York, 1990.
- (35) Henkelman, G.; Arnaldsson, A.; Jónsson, H. *Comput. Mater. Sci.* **2006**, *36*, 354.
- (36) Kresse, G.; Furthmüller, J. *Phys. Rev. B* **1996**, *54*, 11169.
- (37) Kresse, G.; Joubert, D. *Phys. Rev. B* **1999**, *59*, 1758.
- (38) Blöchl, P. E. *Phys. Rev. B* **1994**, *50*, 17953.
- (39) Perdew, J. P. B., K.; Ernzerhof, M. *Phys. Rev. Lett.* **1996**, *77*, 3865.
- (40) Monkhorst, H. J.; Pack, J. D. *Phys. Rev. B* **1976**, *13*, 5188.
- (41) Methfessel, M.; Paxton, A. T. *Phys. Rev. B* **1989**, *40*, 3616.
- (42) Shafai, G.; Hong, S.; Bertino, M.; Rahman, T. S. *J. Phys. Chem. C* **2009**, *113*, 12072.
- (43) Chang, F.-W.; Yu, H.-Y.; Selva Roselin, L.; Yang, H.-C. *Appl. Catal., A* **2005**, *290*, 138.
- (44) Haubrich, J.; Kaxiras, E.; Friend, C. M. *Chem.–Eur. J.* **2011**, *17*, 4496.
- (45) Chretien, S.; Metiu, H. *J. Chem. Phys.* **2007**, *126*, 104701.
- (46) Chretien, S.; Metiu, H. *J. Chem. Phys.* **2007**, *127*, 084704.
- (47) Concepción, P.; Carretin, S.; Corma, A. *Appl. Catal., A* **2006**, *307*, 42.
- (48) Hutchings, G. J.; Hall, M. S.; Carley, A. F.; Landon, P.; Solsona, B. E.; Kiely, C. J.; Herzing, A.; Makkee, M.; Moulijn, J. A.; Overweg, A.; Fierro-Gonzalez, J. C.; Guzman, J.; Gates, B. C. *J. Catal.* **2006**, *242*, 71.
- (49) Green, I. X.; Tang, W.; Neurock, M.; Yates, J. T. *Science* **2011**, *333*, 736.
- (50) Remediakis, I. N.; Lopez, N.; Nørskov, J. K. *Angew. Chem., Int. Ed. Engl.* **2005**, *44*, 1824.
- (51) Wang, J. G.; Hammer, B. *Top. Catal.* **2007**, *44*, 49.
- (52) Frondelius, P.; Häkkinen, H.; Honkala, K. *Angew. Chem., Int. Ed.* **2010**, *49*, 7913.